Bone 48 (2011) 443–450

Contents lists available at ScienceDirect

Bone

journal homepage: www.elsevier.com/locate/bone

Contrast-enhanced micro-computed tomography of fatigue microdamage accumulation in human cortical bone

Matthew D. Landrigan [a], Jiliang Li [b], Travis L. Turnbull [a], David B. Burr [c,d], Glen L. Niebur [a], Ryan K. Roeder [a,*]

[a] Department of Aerospace and Mechanical Engineering, University of Notre Dame, Notre Dame, IN 46556, USA
[b] Department of Biology, Indiana University–Purdue University Indianapolis, Indianapolis, IN 46202, USA
[c] Department of Anatomy and Cell Biology, Indiana University School of Medicine, Indianapolis, IN 46202, USA
[d] Department of Orthopaedic Surgery, Indiana University School of Medicine, Indianapolis, IN 46202, USA

ARTICLE INFO

Article history:
Received 20 July 2010
Revised 22 September 2010
Accepted 8 October 2010
Available online 15 October 2010

Edited by: D. Fyhrie

Keywords:
Barium sulfate
Contrast agent
Cortical bone
Fatigue microdamage
Micro-computed tomography

ABSTRACT

Conventional methods used to image and quantify microdamage accumulation in bone are limited to histological sections, which are inherently invasive, destructive, two-dimensional, and tedious. These limitations inhibit investigation of microdamage accumulation with respect to volumetric spatial variation in mechanical loading, bone mineral density, and microarchitecture. Therefore, the objective of this study was to investigate non-destructive, three-dimensional (3-D) detection of microdamage accumulation in human cortical bone using contrast-enhanced micro-computed tomography (micro-CT), and to validate micro-CT measurements against conventional histological methods. Unloaded controls and specimens loaded in cyclic uniaxial tension to a 5% and 10% reduction in secant modulus were labeled with a precipitated $BaSO_4$ stain for micro-CT and basic fuchsin for histomorphometry. Linear microcracks were similarly labeled by $BaSO_4$ and basic fuchsin as shown by backscattered electron microscopy and light microscopy, respectively. The higher X-ray attenuation of $BaSO_4$ relative to the bone extracellular matrix provided enhanced contrast for the detection of damage that was otherwise not able to be detected by micro-CT prior to staining. Therefore, contrast-enhanced micro-CT was able to nondestructively detect the presence, 3-D spatial location, and accumulation of fatigue microdamage in human cortical bone specimens *in vitro*. Microdamage accumulation was quantified on segmented micro-CT reconstructions as the ratio of $BaSO_4$ stain volume (SV) to total bone volume (BV). The amount of microdamage measured by both micro-CT (SV/BV) and histomorphometry (Cr.N, Cr.Dn, Cr.S.Dn) progressively increased from unloaded controls to specimens loaded to a 5% and 10% reduction in secant modulus ($p<0.001$). Group means for micro-CT measurements of damage accumulation were strongly correlated to those using histomorphometry ($p<0.05$), validating the new methods. Limitations of the new methods in the present study included that the precipitated $BaSO_4$ stain was non-specific and non-biocompatible, and that micro-CT measurements exhibited greater variability compared to conventional histology. Nonetheless, contrast-enhanced micro-CT enabled non-destructive imaging and 3-D spatial information, which are not possible using conventional histological methods.

Introduction

Microdamage has been implicated in clinical fracture susceptibility, including stress fractures in active individuals, fragility fractures in the elderly, and the effects of long-term antiresorptive treatments for osteoporosis [1,2]. Microdamage can accumulate in bone tissue with aging [2–6] and/or repetitive mechanical loading, resulting in the degradation of mechanical properties, such as the elastic modulus [5–11] and fracture toughness [6,12,13], among others. The accumulation of fatigue damage is typically measured mechanically, by a reduction in modulus or stiffness [8–12,14,15], and/or histologically, by microcrack density (Cr.Dn), microcrack length (Cr.Ln.), microcrack surface density (Cr.S.Dn), and diffuse damage [3–16].

Conventional methods used to image and quantify microdamage accumulation in bone are limited to histological sections, which are inherently invasive, destructive, two-dimensional (2-D), and tedious [17]. These methods include: transmitted light or epifluorescence microscopy using basic fuchsin stain [18–21]; epifluorescence microscopy using chelating fluorochromes [22–25]; and backscattered electron microscopy using a lead-uranyl acetate stain [26]. The various contrast agents are used to aid detection of microdamage and differentiate artifactual damage created during specimen preparation. Laser scanning confocal microscopy of damaged tissue labeled with fluorochromes provided enhanced depth of focus for three-dimensional (3-D) imaging [27,28], but remained limited to histological

* Corresponding author. Department of Aerospace and Mechanical Engineering, Bioengineering Graduate Program, 148 Multidisciplinary Research Building, University of Notre Dame, Notre Dame, IN 46556, USA. Fax: +1 574 631 2144.
E-mail address: rroeder@nd.edu (R.K. Roeder).

8756-3282/$ – see front matter © 2010 Elsevier Inc. All rights reserved.
doi:10.1016/j.bone.2010.10.160

sections. Serial sectioning of damaged tissue labeled with fluorochromes enabled 3-D images to be reconstructed from 2-D serial images [29,30], but is destructive and labor intensive. The above limitations associated with conventional histological methods inhibit investigation of microdamage accumulation with respect to volumetric spatial variation in mechanical loading, bone mineral density, and microarchitecture. Moreover, a non-destructive, 3-D method for damage assessment could reduce the time and labor required for current histological methods.

Recent studies have begun to investigate methods for non-destructive, 3-D detection and imaging of microdamage in bone tissue. Fatigue microdamage generated in a rat forelimb was detected *in vivo* by positron emission tomography (PET) using a sodium fluoride ($Na^{18}F$) tracer [31,32], but may be limited in specificity due to the concomitant influence of metabolic activity. X-ray tomography using high energy, monochromatic synchrotron radiation has sufficient resolution to directly image microcracks in bone tissue [33–36], but may embrittle the tissue [36] and is neither readily available nor amenable to imaging large numbers of tissue specimens that are relatively large in size. Therefore, contrast agents have been investigated to enable the use of lower resolution, but commercially available, micro-computed tomography (micro-CT) instruments.

Micro-CT has been investigated for the detection of microdamage *in vitro* using iodinated molecules [17,37], precipitated lead sulfide [38,39], precipitated barium sulfate ($BaSO_4$) [40–42], and functionalized gold nanoparticles [43–45] as contrast agents with higher X-ray attenuation than the extracellular matrix of bone. Lead-based stains were adopted from prior use on 500 μm thick cortical bone sections for histology using electron microscopy [26] and were demonstrated as a micro-CT contrast agent in human femoral trabecular bone specimens which typically exhibit 100–200 μm thick trabeculae [39], but exhibited poor penetration into bulk (4 mm thick) cortical bone specimens [38]. Moreover, lead salts are among the most severe chemical hazards for human health and the environment [46]. Therefore, a new approach was developed for staining by $BaSO_4$ precipitation within damaged tissue, cracks, and vasculature, which was verified by backscattered electron imaging and energy dispersive spectroscopy [40–42]. Damage accumulation that was localized ahead of a notch in bovine cortical bone beams loaded in cyclic four-point bending was stained *in vitro* by precipitation of $BaSO_4$ and imaged using micro-CT [40]. However, the 3-D spatial location of damage accumulation ahead of the notch was to be expected *a priori* and micro-CT measurements were not validated by histology.

Therefore, the objectives of this study were to: (1) detect the 3-D spatial location and quantify the amount of microdamage accumulation within a uniformly stressed volume of human cortical bone using contrast-enhanced micro-CT with a precipitated $BaSO_4$ stain; and (2) validate micro-CT measurements against conventional histological methods. Human cortical bone specimens were loaded in cyclic uniaxial tension to predetermined levels of secant modulus degradation, which was correlated with the level of damage measured by micro-CT and conventional histology on specimens stained with $BaSO_4$ and basic fuchsin, respectively.

Materials and methods

Specimen preparation

Ninety specimens were sectioned from the femoral mid-diaphysis of three Caucasian men (62, 62 and 65 years of age) presenting no medical history of skeletal pathology or trauma. All tissues were obtained with donor's consent (National Disease Research Interchange, Philadelphia, PA) and all protocols were approved by the Notre Dame Human Subjects Institutional Review Board. Cylindrical specimens were machined to a 2.5 mm diameter by 5 mm gauge length on a computer numerical controlled lathe (4500 Series, Sherline Products, Inc., Vista, CA). Specimens were randomly assigned to six experimental groups ($n = 15$/group), comprising an unloaded control and two mechanically loaded groups for both micro-CT and conventional histology. Specimens were wrapped in gauze, hydrated in phosphate buffered saline (PBS), and stored at −20 °C in airtight containers during interim periods.

Fatigue loading

Mechanically loaded specimens were subjected to cyclic uniaxial tension ($R = 0$) at 2 Hz under load control on an electromagnetic test instrument (ElectroForce 3300, Bose Corp., Eden Prairie, MN) while hydrated with a de-ionized (DI) water drip at ambient temperature until achieving a 5% or 10% reduction in the secant modulus. Note that loading was completed within a relatively short duration (within 18 h for 26 specimens and within 5 days for 4 specimens), allowing the use of a DI water drip without significant effect on the tissue. The secant modulus was measured as the slope of the line connecting the minimum and maximum load and displacement for a given loading cycle. Displacements were measured via a cross-head linear variable displacement transducer (±0.025 mm sensitivity), which was verified against measurements using an extensometer.

Specimens were first preconditioned at 60 MPa for 20 cycles and the initial secant modulus was measured as the average of the first 10 cycles. Maximum fatigue load levels were normalized to an initial maximum strain of 6400 ± 300 microstrain using the initial secant modulus. The secant modulus degradation during fatigue loading was measured as the percent reduction in secant modulus at a given number of loading cycles relative to the initial secant modulus. For specimens loaded to a 5% reduction in secant modulus, the average of five cycles was taken in order to filter noise and prevent premature stoppage of the test. Specimens loaded to a 10% reduction in secant modulus did not require averaging because a 10% reduction in secant modulus typically coincided with fatigue crack propagation prior to fracture. Thus, averaging multiple cycles would have resulted in catastrophic failure of many specimens. Finally, the total number of loading cycles was recorded upon reaching the predetermined secant modulus degradation for each specimen.

Barium sulfate staining and micro-CT

Unloaded controls and specimens loaded to a 5% and 10% reduction in secant modulus were stained by $BaSO_4$ precipitation. Specimens were soaked in a solution of equal parts buffered saline, acetone, and 0.5 M $BaCl_2$ (certified ACS crystal, Fisher Scientific, Fair Lawn, NJ) in DI water for 3 days, followed by a solution of equal parts buffered saline, acetone, and 0.5 M $NaSO_4$ (anhydrous powder, Fisher Scientific, Fair Lawn, NJ) in DI water for 3 days, both under vacuum (~50 mm Hg). Specimens were rinsed with DI water after each step to minimize ions or particles on specimen surfaces. The staining mechanism was a precipitation reaction where $BaCl_2(aq) + Na_2SO_4(aq) \rightarrow BaSO_4(s) + 2NaCl(aq)$. Barium and sulfate ions diffused into and concentrated within void space in the tissue–e.g., microcracks, damaged tissue and vasculature–which provided an abundance of heterogeneous nucleation sites for precipitation on tissue surfaces [40].

The entire gauge length of each stained specimen was imaged by micro-CT (μCT-80, Scanco Medical AG, Brüttisellen, Switzerland) at 10 μm resolution, 70 kVp voltage, 113 μA current, and 400 ms integration time with slices taken perpendicular to the longitudinal specimen axis. Note that selected specimens were also imaged by micro-CT after mechanical loading but prior to staining in order to determine whether micro-CT could detect microdamage without the contrast agent. Grayscale images were smoothed by a Gaussian filter with sigma = 1.5 and support = 3. The ratio of $BaSO_4$ stain volume (SV) to total bone volume (BV), SV/BV, was adopted as a measure of

damage. High intensity voxels representative of SV were segmented at a constant global threshold of 490, corresponding to a mean linear attenuation coefficient of 3.92 cm^{-1} or ~1890 mg hydroxyapatite per cubic centimeter (mg HA/cm^3), which was well above the tissue mineral density of human cortical bone [47]. Low intensity voxels representative of Haversian porosity were segmented at a constant global threshold of 270 (2.16 cm^{-1} or ~839 mg HA/cm^3) prior to staining and 290 (2.32 cm^{-1} or ~924 mg HA/cm^3) after staining. These thresholds were shown to provide similar measurements of porosity for the same specimen before and after staining due to an overall shift in image intensity. BV was measured from all voxels above the Haversian porosity threshold. In order to minimize the effect of non-specific $BaSO_4$ staining on specimen free surfaces, a cylindrical image subregion was analyzed with a radius reduced by 100 μm (10 voxels) from the specimen perimeter. The above parameters were determined to provide an optimal balance of sensitivity and noise suppression after a systematic evaluation described in detail elsewhere [48].

After micro-CT, selected specimens were prepared for scanning electron microscopy (SEM). These specimens were dehydrated in a graded series of alcohol solutions, dried overnight in an oven at 90 °C, embedded in poly(methyl methacrylate), sectioned longitudinally with a low-speed diamond wafer saw, polished with a series of diamond compounds to a 1 μm finish, washed with ethanol, dried overnight in an oven at 90 °C, and coated with Au-Pd by sputter deposition. Specimens were imaged using backscattered electron imaging (BEI) at an accelerating voltage of 20 kV and a working distance of 7 mm (Evo 50, LEO Electron Microscopy Ltd., Cambridge UK). Note that image contrast from backscattered electrons is primarily due to compositional differences in atomic number, with an increasing atomic number resulting in increased intensity. The elemental composition of the stain was verified by electron probe microanalysis (EPMA) using energy dispersive spectroscopy (EDS) (INCA x-sight model 7636, Oxford Instruments America, Concord, MA).

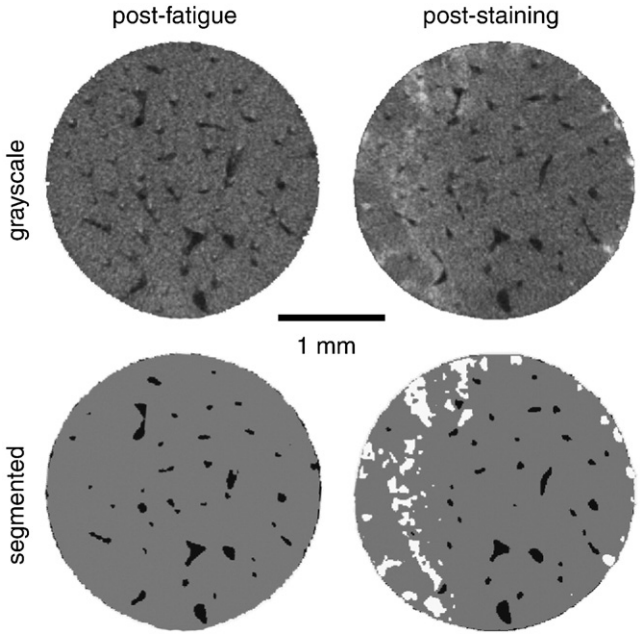

Fig. 1. Grayscale and segmented micro-CT images of the same specimen cross-section (2.5 mm diameter) after loading to a 10% reduction in secant modulus but prior to staining (post-fatigue), and after staining with $BaSO_4$ (post-staining), showing enhanced contrast (bright voxels) for the detection of damage that was not able to be detected prior to staining.

Validation by basic fuchsin staining

For validation by conventional histology, specimens were stained *en bloc* under vacuum (15–20 mm Hg) by 1% basic fuchsin in a graded series of alcohol solutions (80%, 95%, and 100% ethanol) which were changed after 2 h in each [20]. After staining, specimens were rinsed in 100% ethanol, followed by 100% methyl methacrylate, for 4 h each under vacuum and embedded in poly(methyl methacrylate) with 3% dibutyl phthalate. Longitudinal serial sections, 80 μm in thickness, were prepared using a diamond wire saw (Delaware Diamond Knives, Wilmington, DE) and 5–7 sections within the gauge section of each specimen were assessed histologically for microdamage. Note that this technique is able to discriminate artifactual damage caused by histological preparation processes from prior fatigue microdamage [19].

Histomorphometry was carried out by a single individual blinded to group affiliation using transmitted light microscopy (Optiphot 2, Nikon) with a semiautomatic digitizing system (OSTEO 7.20.10, Bioquant Image Analysis Corp., Nashville, TN). Stained microcracks were identified by shape, depth of field, and permeation of the stain into crack surfaces. The crack density was measured as the number of linear microcracks normalized to bone area (Cr.Dn = Cr.N/bone area, #/mm^2). Crack lengths (Cr.Le, μm) were measured and the mean Cr.Le was used to calculate the crack surface density (Cr.S.Dn, μm/mm^2) as the product of Cr.Dn and mean Cr.Le.

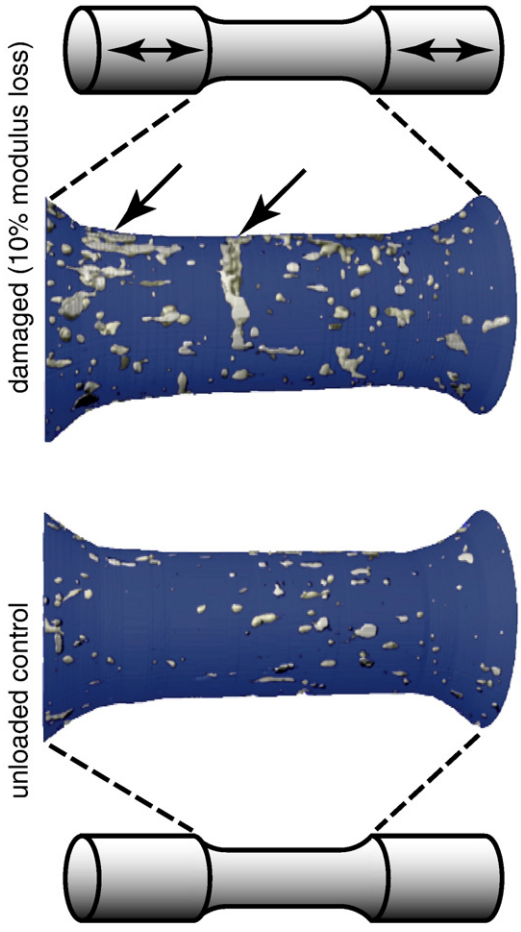

Fig. 2. Segmented, 3-D micro-CT reconstructions of the entire gauge section (2.5 mm in diameter by 5 mm in length) for an unloaded control specimen compared to a specimen loaded in cyclic uniaxial tension to a 10% reduction in secant modulus, showing the ability of micro-CT to detect spatial variation in damage accumulation. Arrows highlight regions of concentrated $BaSO_4$ staining characteristic of fatigue damage and/or propagating microcracks.

Statistical methods

Micro-CT (SV/BV) and histological (Cr.N, Cr.Le, Cr.Dn, and Cr.S.Dn) measurements of microdamage exhibited non-homogeneous variances. Therefore, experimental groups were compared using Kruskal–Wallis non-parametric analysis of variance (ANOVA) and post-hoc comparisons were performed using Mann–Whitney *U*-tests with a Bonferroni correction for multiple comparisons (JMP 8, SAS Institute Inc., Cary, NC). Linear least squares regression was used to correlate SV/BV, Cr.N, Cr.Dn, Cr.S.Dn, the number of loading cycles, and Haversian porosity. Spearman's rho was used to correlate the ranked group means for micro-CT (SV/BV) and histological measurements (Cr.N, Cr.Dn, and Cr.S.Dn) of microdamage accumulation. Eta-squared (η^2) was calculated as a correlation coefficient for the variance of histological measurements (Cr.N, Cr.Dn, and Cr.S.Dn) able to be predicted by SV/BV means. The level of significance for all tests was set at 0.05.

Results

The presence and spatial location of fatigue microdamage was non-destructively detected by micro-CT after staining with $BaSO_4$. Grayscale and segmented micro-CT images of the same specimen cross-section, after loading to a 10% reduction in secant modulus and after $BaSO_4$ staining (post-staining), showed enhanced contrast (bright voxels) for microdamage that was not able to be detected by micro-CT prior to staining (post-fatigue) (Fig. 1). Segmented, 3-D reconstructions of the entire gauge section showed the ability of micro-CT to detect spatial variation in damage accumulation (Fig. 2). Unloaded control specimens revealed non-specific $BaSO_4$ staining on free surfaces and within vasculature. Specimens loaded in cyclic uniaxial tension typically exhibited at least one distinct region of concentrated $BaSO_4$ stain which appeared characteristic of fatigue damage and/or propagating microcracks (e.g., see arrows in Fig. 2). See the Appendix for movies showing cross-sectional grayscale image stacks using contrast-enhanced micro-CT for representative specimens from the unloaded control group and groups loaded to a 5% and 10% reduction in secant modulus.

Linear microcracks generated by cyclic uniaxial tension were similarly labeled by $BaSO_4$ (bright) and basic fuchsin (violet) as shown by backscattered electron microscopy and light microscopy, respectively, on separate specimens from paired experimental groups (Fig. 3). Therefore, bright voxels detected by micro-CT were confirmed by backscattered electron microscopy to be microcracks and/or diffuse damage labeled with $BaSO_4$ (Figs. 3a and 4a). Moreover, EDS confirmed elevated levels of Ba in stained versus unstained regions of tissue (Fig. 4b).

The amount of microdamage increased from the unloaded control group to groups loaded to a 5% and 10% reduction in secant modulus for both micro-CT (SV/BV) and histological (e.g., Cr.Dn) measurements of microdamage ($p<0.001$, Kruskal–Wallis) (Fig. 5). All differences between experimental groups were statistically significant ($p<0.05$, Mann–Whitney *U*-test). For example, SV/BV and Cr.Dn for specimens loaded to a 10% reduction in secant modulus exhibited a four- and ten-fold increase over controls, respectively. Histological measurements for the crack number (Cr.N) and crack surface density (Cr.S.Dn) exhibited similar trends as Cr.Dn (Table 1). However, the mean crack length (Cr.Le) was not statistically different between controls and specimens loaded to a 5% reduction in secant modulus, but was increased for a 10% reduction in secant modulus (Table 1).

The accumulation of microdamage measured by micro-CT (SV/BV) was correlated with Cr.Dn (Fig. 6), Cr.N, and Cr.S.Dn measured by conventional histology ($p<0.05$, Spearman's rho) allowing prediction of Cr.Dn, Cr.N, and Cr.S.Dn from SV/BV group means ($\eta^2 = 0.78$, 0.78, and 0.65, respectively). SV/BV was not correlated with the level of Haversian porosity ($p = 0.87$). The overall mean (±standard

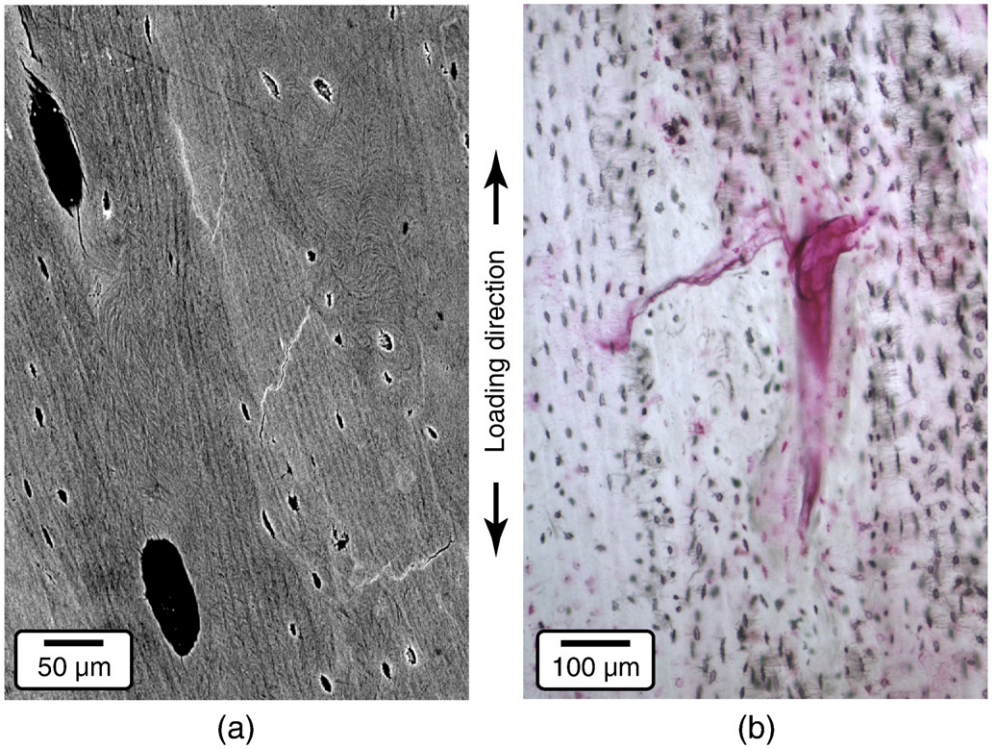

Fig. 3. Representative (a) backscattered SEM and (b) transmitted light micrographs for specimens loaded in cyclic uniaxial tension to a 5% reduction in secant modulus, showing transverse linear microcracks within interstitial tissue similarly labeled by $BaSO_4$ (bright) and basic fuchsin (violet), respectively.

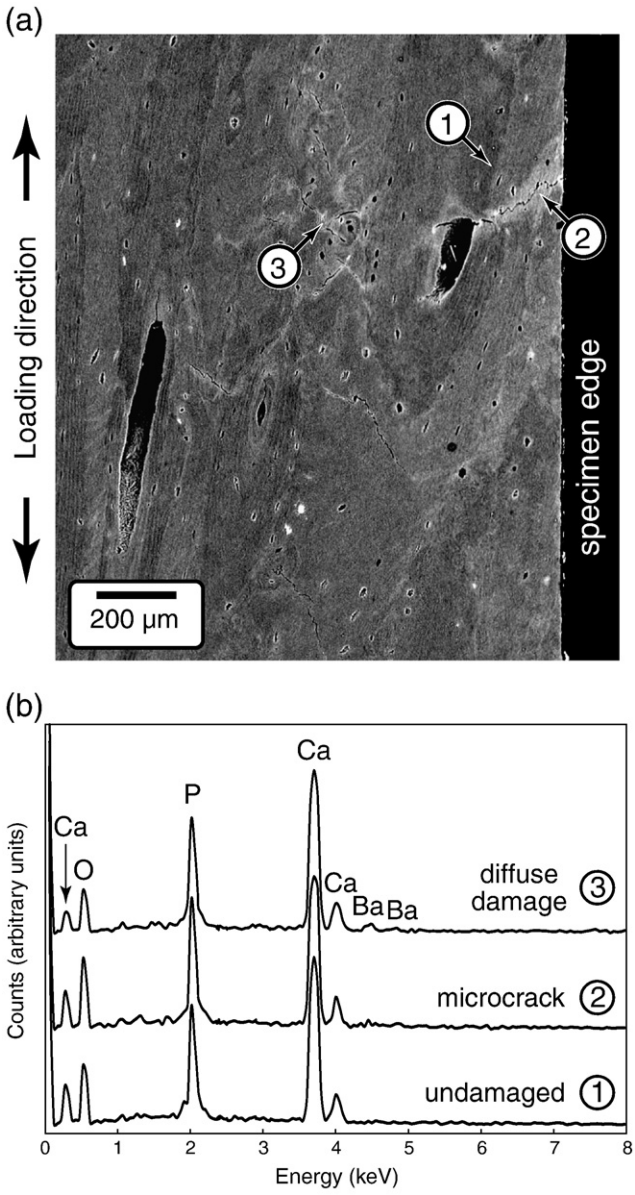

Fig. 4. (a) Backscattered SEM micrograph for a specimen loaded in cyclic uniaxial tension to a 10% reduction in secant modulus, showing (2) a microcrack that propagated between the specimen edge and a Haversian canal and (3) diffuse damage accumulated in interstitial tissue, both labeled by $BaSO_4$ (bright). (b) The elemental composition measured using EDS showed elevated levels of Ba associated with (2) linear microcracks and (3) diffuse damage compared to (1) undamaged tissue.

deviation) level of Haversian porosity was 2.54 (1.46) %, and differences between experimental groups were not statistically significant ($p=0.70$ Kruskal–Wallis). In mechanically loaded specimens, SV/BV was not correlated with the number of loading cycles ($p=0.16$), but the number of loading cycles exhibited a weak, negative correlation ($p<0.05$, $R^2=0.15$) with the level of Haversian porosity.

Discussion

The 3-D spatial location of microdamage within a uniformly stressed volume of human cortical bone was non-destructively detected and quantified *in vitro* using contrast-enhanced micro-CT with a precipitated $BaSO_4$ stain. A previous study, using similar staining and imaging methods, demonstrated the detection of microdamage that was localized ahead of a notch in bovine cortical bone

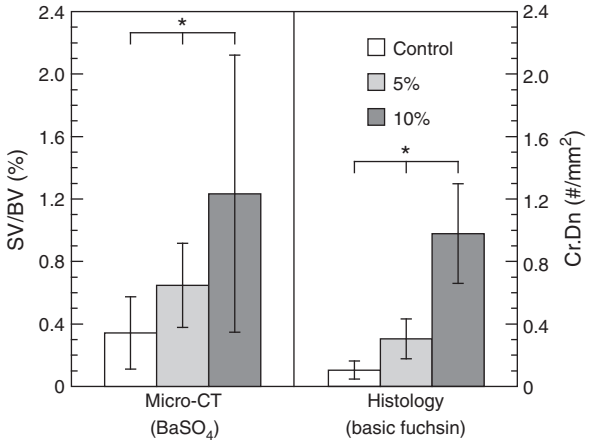

Fig. 5. The amount of microdamage increased from the unloaded control group to groups loaded to a 5% and 10% reduction in secant modulus for both micro-CT (SV/BV) and histological (Cr.Dn) measurements of microdamage ($p<0.001$, Kruskal–Wallis). Error bars span one standard deviation. Asterisks denote statistically significant differences between groups ($p<0.05$, Mann–Whitney *U*-test).

beams loaded in cyclic four-point bending [40]. However, the spatial location of microdamage accumulation was known *a priori* due to the use of notched beams, and the quantification of microdamage accumulation rapidly saturated due to crack initiation from the notch and the use of displacement-controlled fatigue. In the present study, the use of load-controlled fatigue on a uniformly stressed volume demonstrated the feasibility of detecting of the 3-D spatial location (Figs. 1–2) and progressive accumulation (Fig. 5) of microdamage in human cortical bone. Of the 15 specimens per experimental group, 12 and 14 specimens loaded in cyclic uniaxial tension to a 5% and 10% reduction in secant modulus, respectively, exhibited at least one distinct region of concentrated $BaSO_4$ stain which appeared indicative of fatigue damage and/or propagating microcracks (e.g., see arrows in Fig. 2). Regions of concentrated $BaSO_4$ stain were located near the center or ends of the gauge length in 13 specimens each, and the mean SV/BV was not statistically different between each location for specimens loaded to either a 5% and 10% reduction in secant modulus ($p=0.4$ and 0.9, respectively, *t*-test). Thus, tissue in the specimen gauge section was confirmed to be uniformly stressed and damage accumulated with equal probability at any location within the tissue volume.

$BaSO_4$ staining provided enhanced contrast for the detection of damage that was otherwise not able to be detected using a polychromatic, cone-beam micro-CT scanner at 10 μm resolution (Fig. 1). Typical microcracks in cortical bone tissue are elliptical, with a width and length on the order of 100–500 μm [28,30], and a thickness on the order of 1 μm [18,26,35]. The thickness of microcracks in this study was also observed by electron and optical microscopy to be on the order of 1 μm (Figs. 3 and 4a), which was well below the 10 μm voxel size of the micro-CT scanner. $BaSO_4$ precipitation within microcracks, and penetration into adjacent tissue, enhanced the intensity of voxels in micro-CT due to the higher X-ray attenuation of $BaSO_4$ relative to the extracellular matrix (Fig. 4) [40–42]. Moreover,

Table 1
The mean (±standard deviation) crack number (Cr.N), crack length (Cr.Le), crack density (Cr.Dn), and crack surface density (Cr.S.Dn) for the unloaded control group and groups loaded to a 5% and 10% reduction in secant modulus using conventional histology after staining by basic fuchsin. Groups not connected by the same superscript letter exhibited statistically significant differences ($p<0.05$, Mann–Whitney *U*-test).

Group	Cr.N (#)	Cr.Le (μm)	Cr.Dn (#/mm²)	Cr.S.Dn (μm/mm²)
Control	5 (3)[a]	84 (10)[a]	0.10 (0.06)[a]	9 (5)[a]
5%	14 (6)[b]	85 (21)[a]	0.30 (0.13)[b]	26 (11)[b]
10%	44 (13)[c]	100 (19)[b]	0.98 (0.32)[c]	101 (48)[c]

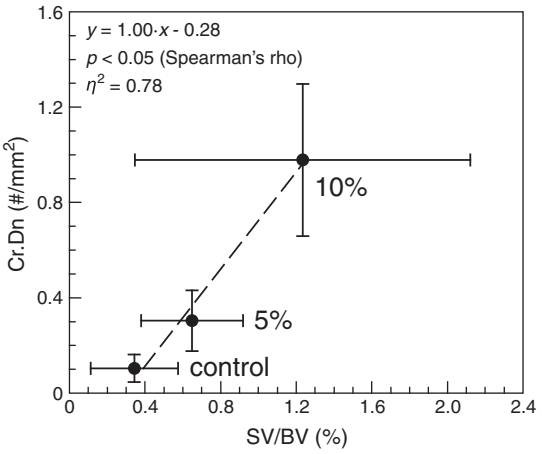

Fig. 6. The accumulation of microdamage measured by micro-CT (SV/BV) was correlated with the microcrack density (Cr.Dn) measured by conventional histology ($p<0.05$, Spearman's rho) allowing prediction of Cr.Dn from SV/BV group means ($\eta^2=0.78$). Data points show the mean and one standard deviation ($n=15$/group) for the unloaded control group and groups loaded to a 5% and 10% reduction in secant modulus.

artifactual microcracks resulting from subsequent histological specimen preparation were not labeled by $BaSO_4$ and were therefore able to be distinguished from pre-existing microcracks, since $BaSO_4$ staining was conducted on tissue specimens *en bloc* immediately after mechanical loading.

Contrast-enhanced micro-CT was able to detect and quantify the progressive accumulation of fatigue microdamage from unloaded control specimens to those loaded to a 5% and 10% reduction in secant modulus (Fig. 5). Group means for micro-CT measurements of damage accumulation (SV/BV) exhibited a strong correlation with those using histomorphometry (e.g., Cr.Dn), validating the new methods (Fig. 6). However, note that this correlation may not be generally applicable for prediction of Cr.Dn from SV/BV since measurements of the SV are dependent on the staining and imaging methods, as described in further detail below.

Post hoc power analysis using the root mean square error, total number of specimens, and $\alpha=0.05$ for the unloaded control specimens and those loaded to a 5% reduction in secant modulus resulted in a power of 0.89 for a difference of 0.302 between the group means for SV/BV, which corresponded to an 87% (1.9-fold) increase in SV/BV over the unloaded control group. For the same level of power, *post hoc* power analysis suggested that histology (Cr.Dn) was able to detect a 115% increase (2.2-fold) in Cr.Dn over the unloaded control group. Therefore, the level of damage incurred by a 5% reduction in secant modulus was just above the minimum level that could be expected to be detected by contrast-enhanced micro-CT for the sample size and methods used in this study, and the sensitivity of contrast enhanced micro-CT was not unlike that that exhibited by conventional histological measurements.

Histological measurements of microdamage have been correlated to a reduction in modulus (or stiffness) in surprisingly few studies and with varied results. In whole canine femora loaded in cyclic four-point bending to a 5–45% reduction in stiffness, microdamage was not observed histologically until a 15% reduction in stiffness [9]. The crack area (Cr.Ar) was positively and significantly correlated with the stiffness degradation, but other histological measures (Cr.Dn, Cr.Le, etc.) did not exhibit a statistically significant difference from unloaded control specimens nor a correlation with the stiffness degradation [9]. In human femoral cortical bone specimens subjected to tensile overloading to a 0–10% reduction in elastic modulus, Cr.N and Cr.Le exhibited a positive but weak ($R^2=0.15$–0.24) correlation with the modulus degradation [8]. Whole rat ulnae loaded in cyclic bending exhibited a statistically significant increase in Cr.Dn, Cr.Le, and Cr.S.Dn in loaded groups compared to unloaded controls, but differences between groups loaded to a 20% and 40% reduction in stiffness were not statistically significant [10]. Bovine tibial cortical bone specimens loaded in cyclic uniaxial compression exhibited a statistically significant increase in Cr.Dn, Cr.Le, and Cr.S.Dn for specimens loaded to a 10% reduction in elastic modulus compared to unloaded controls, as well as interesting trends with the number of loading cycles [7]. Finally, bovine tibial cortical bone specimens loaded in cyclic four-point bending exhibited a statistically significant increase in Cr.Dn for compressive loading, but no difference for tensile loading, between a 20% and 50% degradation in the elastic modulus determined using linear elastic beam theory [12]. In light of these prior studies, the strong correlation of both micro-CT (SV/BV) and histological (Cr.N, Cr.Dn, Cr.S.Dn) measurements of microdamage with the modulus degradation (Fig. 5) in the present study was itself a significant result. A reduction in secant modulus greater than 10% could not be reliably achieved prior to fracture of the specimens in the present study, which was similar to the most closely related prior study [7]. The wide variation in mechanical degradation observed amongst the other studies is most likely due to differences in loading mode [12] and tissue source, as well as systematic experimental errors [15].

Unloaded control specimens exhibited a mean microcrack length and density (Table 1) that was comparable to prior measurements for microdamage in human femoral cortical bone tissue from donors of similar age [3,5,8]. Specimens loaded to a 5% reduction in secant modulus primarily exhibited transverse microcracks in interstitial tissue, which terminated at cement lines, and longitudinal microcracks along cement lines (Fig. 4). Specimens loaded to a 10% reduction in secant modulus exhibited transverse propagating microcracks or fatigue cracks (e.g., Fig. 4a). These cracks appeared to originate at the specimen surface and propagate inward, normal to the direction of loading, as expected for fatigue failure in cyclic uniaxial tension. The number of loading cycles required to reach the designated reduction in secant modulus for loaded specimens exhibited a negative correlation with the level of Haversian porosity, suggesting that Haversian porosity may have provided stress concentrations for primary crack initiation and/or secondary crack initiation ahead of a propagating microcrack (Fig. 3b) [49] especially when located near the specimen surface (Fig. 4a).

This study was not without several limitations. Staining by $BaSO_4$ precipitation was non-specific for microdamage, including all void spaces, such as vasculature and free surfaces, and the staining solutions were not biocompatible. Therefore, the new methods demonstrated in this study are limited to use *in vitro*. However, functionalized gold [43–45] and $BaSO_4$ nanoparticles are being investigated for a deliverable, targeted X-ray contrast agent for damaged bone tissue.

The amount of damage measured by micro-CT (SV/BV) exhibited greater variability, and decreased relative differences between experimental groups, compared to conventional histology (Cr.Dn) (Fig. 5). The most likely contributing factors were the relatively lower resolution of micro-CT and non-specific $BaSO_4$ staining. Unloaded control specimens exhibited scattered, small volumes of $BaSO_4$ staining on free surfaces and within vasculature (Fig. 2). However, SV/BV was not correlated with the amount of Haversian porosity in individual specimens. Further work is required to determine whether SV/BV would be influenced by higher levels of Haversian porosity than that exhibited by the tissue specimens in this study. Alternatively, a segmented reconstruction of Haversian porosity imaged prior to staining could be overlayed or subtracted from segmented reconstructions imaged after staining.

The subregion and threshold for analysis and segmentation, respectively, required careful selection. A parametric study was used to determine the effects of the image subregion size and threshold value on the magnitude and variability of SV/BV [48]. The effects of non-specific staining on the specimen free surfaces were minimized

by analyzing a subregion with a radius reduced by 100 μm (10 voxels) from the specimen perimeter. However, the removal of this tissue from analysis also excluded SV that was due to microdamage and may have contributed to the increased variability in SV/BV with an increased reduction in secant modulus, since propagating microcracks were typically observed at or near the specimen surface. The optimal threshold ($3.92\ cm^{-1}$) for segmenting the SV corresponded to an equivalent density of ~1890 mg hydroxyapatite per cubic centimeter, which was well above the tissue mineral density of human cortical bone [47].

Finally, microdamage accumulation was quantified by micro-CT as SV/BV, but a true crack density and crack dimensions could not be measured. The resolution and absorption contrast limits of a polychromatic, cone-beam micro-CT with 10 μm resolution did not allow imaging of individual microcracks or discrimination between microdamage and non-specific staining, though the latter may be feasible using morphological criteria. The use of higher resolution and/or monochromatic radiation could enable dimensional measurements of microcracks, but only at the cost of sample volume and radiation dose. However, SV/BV was shown to be strongly correlated with the crack density measured histologically (Fig. 6). Therefore, a greater impact for contrast-enhanced micro-CT could be realized by extension to instruments with lower resolution and lower radiation doses in order to enable non-invasive, 3-D detection of microdamage in whole bones using preclinical instruments for small animals, or even clinical instruments.

In conclusion, contrast-enhanced micro-CT was able to detect the presence, spatial location, and progressive accumulation of fatigue microdamage in human cortical bone specimens *in vitro* using a precipitated $BaSO_4$ stain, and was validated against conventional histological methods using basic fuchsin. Limitations of the new methods in the present study included that the precipitated $BaSO_4$ stain was non-specific and non-biocompatible, and that micro-CT measurements exhibited greater variability compared to conventional histology. Nonetheless, contrast-enhanced micro-CT enabled non-destructive imaging and 3-D spatial information, which are not possible using conventional histological methods. Therefore, contrast-enhanced micro-CT is immediately useful in the study of bone tissue mechanics, including the etiology of fatigue and fragility fractures.

Supplementary materials related to this article can be found online at doi:10.1016/j.bone.2010.10.160.

Acknowledgments

This research was supported by the U.S. Army Medical Research and Materiel Command (W81XWH-06-1-0196) through the Peer Reviewed Medical Research Program (PR054672).

References

[1] Chapurlat BD, Delmas PD. Bone microdamage: a clinical perspective. Osteoporos Int 2009;20:1299–308.
[2] Burr DB, Forwood MR, Fyhrie DP, Martin RB, Schaffler MB, Turner CH. Bone microdamage and skeletal fragility in osteoporotic and stress fractures. J Bone Miner Res 1997;12:6–15.
[3] Norman TL, Wang Z. Microdamage of human cortical bone: incidence and morphology in long bones. Bone 1997;20:375–9.
[4] Schaffler MB, Choi K, Milgrom C. Aging and matrix microdamage accumulation in human compact bone. Bone 1995;17:521–5.
[5] Sobelman OS, Gibeling JC, Stover SM, Hazelwood SJ, Yeh OC, Shelton DR, Martin RB. Do microcracks decrease or increase fatigue resistance in cortical bone? J Biomech 2004;37:1295–303.
[6] Zioupos P. Accumulation of *in-vivo* fatigue microdamage and its relation to biomechanical properties in ageing human cortical bone. J Microsc 2001;201(Pt 2):270–8.
[7] O'Brien FJ, Taylor D, Lee TC. Microcrack accumulation at different intervals during fatigue testing of compact bone. J Biomech 2003;36:973–80.
[8] Akkus O, Knott DF, Jepsen KJ, Davy DT, Rimnac CM. Relationship between damage accumulation and mechanical property degradation in cortical bone: microcrack orientation is important. J Biomed Mater Res 2003;65A:482–8.
[9] Burr DB, Turner CH, Naick P, Forwood MR, Ambrosius W, Hasan MS, Pidaparti R. Does microdamage accumulation affect the mechanical properties of bone? J Biomech 1998;31:337–45.
[10] Danova NA, Colopy SA, Radtke CL, Kalscheur VL, Markel MDR, Vanderby J, McCabe RP, Escarcega AJ, Muir P. Degradation of bone structural properties by accumulation and coalescence of microcracks. Bone 2003;33:197–205.
[11] Forwood MR, Parker AW. Microdamage in response to repetitive torsional loading in the rat tibia. Calcif Tissue Int 1989;45:47–53.
[12] Diab T, Vashishth D. Effects of damage morphology on cortical bone fragility. Bone 2005;37:96–102.
[13] Norman TL, Yeni YN, Brown CU, Wang X. Influence of microdamage on fracture toughness of the human femur and tibia. Bone 1998;23:303–6.
[14] Boyce TM, Fyhrie DF, Glotkowski MC, Radin EL, Schaffler MB. Damage type and strain mode associations in human compact bone bending fatigue. J Orthop Res 1998;16:322–9.
[15] Landrigan MD, Roeder RK. Systematic error in mechanical measures of damage during four-point bending fatigue of cortical bone. J Biomech 2009;42:1212–7.
[16] Diab T, Condon KW, Burr DB, Vashishth D. Age-related change in the damage morphology of human cortical bone and its role in bone fragility. Bone 2006;38:427–31.
[17] Lee TC, Mohsin S, Taylor D, Parkesh R, Gunnlaugsson T, O'Brien FJ, Giehl M, Gowin W. Detecting microdamage in bone. J Anat 2003;203:161–72.
[18] Frost HM. Presence of microscopic cracks in vivo in bone. Henry Ford Hosp Med Bull 1960;8:25–35.
[19] Burr DB, Stafford T. Validity of the bulk-staining technique to separate artefactual from *in vivo* bone microdamage. Clin Orthop Relat Res 1990;260:305–8.
[20] Burr DB, Hooser M. Alterations to the en bloc basic fuchsin staining protocol for the demonstration of microdamage produced in vivo. Bone 1995;17:431–3.
[21] Lee TC, Myers ER, Hayes WC. Fluorescence-aided detection of microdamage in compact bone. J Anat 1998;193:179–84.
[22] Lee TC, Arthur TL, Gibson LJ, Hayes WC. Sequential labelling of microdamage in bone using chelating agents. J Orthop Res 2000;18:22–325.
[23] O'Brien FJ, Taylor D, Lee TC. An improved labelling technique for monitoring microcrack growth in compact bone. J Biomech 2002;35:523–6.
[24] Parkesh R, Mohsin S, Lee TC, Gunnlaugsson T. Histological, spectroscopic, and surface analysis of microdamage in bone: toward real-time analysis using fluorescent sensors. Chem Mater 2007;19:1656–63.
[25] Parkesh R, Lee TC, Gunnlaugsson T. Fluorescence imaging of bone cracks (microdamage) using visibly emitting 1, 8-naphthalimide-based PET sensors. Tetrahedron Lett 2009;50:4114–6.
[26] Schaffler MB, Pitchford WC, Choi K, Riddle JM. Examination of compact bone microdamage using back-scattered electron microscopy. Bone 1994;15:483–8.
[27] Zioupos P, Currey JD. The extent of microcracking and the morphology of microcracks in damaged bone. J Mater Sci 1994;29:978–86.
[28] O'Brien FJ, Taylor D, Dickson GR, Lee TC. Visualization of three-dimensional microcracks in compact bone. J Anat 2000;197:413–20.
[29] Bigley RF, Singh M, Hernandez CJ, Kazakia GJ, Martin RB, Keaveny TM. Validity of serial milling-based imaging system for microdamage quantification. Bone 2008;42:212–6.
[30] Mohsin S, O'Brien FJ, Lee TC. Microcracks in compact bone: a three-dimensional view. J Anat 2006;209:119–24.
[31] Li J, Miller MA, Hutchins GD, Burr DB. Imaging bone microdamage in vivo with positron emission tomography. Bone 2005;37:819–24.
[32] Silva MJ, Uthgenannt BA, Rutlin JR, Wohl GR, Lewis JS, Welch MJ. In vivo skeletal imaging of ^{18}F-fluoride with positron emission tomography reveals damage- and time-dependent responses to fatigue loading in the rat ulna. Bone 2006;39:229–36.
[33] Nalla RK, Kruzic JJ, Kinney JH, Ritchie RO. Mechanistic aspects of fracture and R-curve behavior in human cortical bone. Biomaterials 2005;26:217–31.
[34] Thurner PJ, Wyss P, Voide R, Stauber M, Stampanoni M, Sennhauser U, Müller R. Time-lapsed investigation of three-dimensional failure and damage accumulation in trabecular bone using synchrotron light. Bone 2006;39:289–99.
[35] Voide R, Schneider P, Stauber M, Wyss P, Stampanoni M, Sennhauser U, van Lenthe GH, Müller R. Time-lapsed assessment of microcrack initiation and propagation in murine cortical bone at submicrometer resolution. Bone 2009;45:164–73.
[36] Barth HD, Launey ME, MacDowell AA, Ager JW, Ritchie RO. On the effect of X-ray irradiation on the deformation and fracture behavior of human cortical bone. Bone 2010;46:1475–85.
[37] Parkesh R, Lee TC, Gunnlaugsson T, Gowin W. Microdamage in bone: surface analysis and radiological detection. J Biomech 2006;39:1552–6.
[38] Leng H. Micro-computed tomography of microdamage in cortical bone. University of Notre Dame, Notre Dame, IN: Ph.D. Dissertation; 2006.
[39] Tang SY, Vashishth D. A non-invasive in vitro technique for the three-dimensional quantification of microdamage in trabecular bone. Bone 2007;40:1259–64.
[40] Leng H, Wang X, Ross RD, Niebur GL, Roeder RK. Micro-computed tomography of fatigue microdamage in cortical bone using a barium sulfate contrast agent. J Mech Behav Biomed Mater 2008;1:68–75.
[41] Wang X, Masse DB, Leng H, Hess KP, Ross RD, Roeder RK, Niebur GL. Detection of trabecular bone microdamage by micro-computed tomography. J Biomech 2007;40:3397–403.
[42] Landrigan MD, Flatley JC, Turnbull TL, Kruzic JJ, Ferracane JL, Hilton TJ, Roeder RK. Detection of dentinal cracks using contrast-enhanced micro-computed tomography. J Mech Behav Biomed Mater 2010;3:223–7.
[43] Zhang Z, Ross RD, Roeder RK. Preparation of functionalized gold nanoparticles as a targeted X-ray contrast agent for damaged bone tissue. Nanoscale 2010;2:582–6.
[44] Ross RD, Roeder RK. Binding affinity of surface functionalized gold nanoparticles for hydroxyapatite. J Biomed Mater Res, submitted.

[45] Ross RD, Roeder RK. Functionalized gold nanoparticles for targeted labeling of damaged bone tissue in X-ray tomography. Trans Orthop Res Soc 2010;35: 1368.
[46] Swanson MB, Davis GA, Kincaid LE, Schultz TW, Bartness JE, Jones SL, George EL. A screening method for ranking and scoring chemical by potential human health and environmental impacts. Environ Toxicol Chem 1997;16:372–83.
[47] Deuerling JM, Rudy DJ, Niebur GL, Roeder RK. Improved accuracy of cortical bone mineralization measured by polychromatic micro-computed tomography using a novel high mineral density composite calibration phantom. Med Phys 2010;37: 5138–45.
[48] Landrigan MD. Evaluation of methods for measuring microdamage accumulation in cortical bone. University of Notre Dame, Notre Dame, IN: Ph.D. Dissertation; 2009.
[49] Fleck C, Eifler D. Deformation behaviour and damage accumulation of cortical bone specimens from the equine tibia under cyclic loading. J Biomech 2003;36: 179–89.